Chemosphere 239 (2020) 124832

Contents lists available at ScienceDirect

Chemosphere

journal homepage: www.elsevier.com/locate/chemosphere

Waste sludge derived adsorbents for arsenate removal from water

Rahul Kumar [a, b, c, 1], Chan-Ung Kang [a, 1], Dinesh Mohan [b], Moonis Ali Khan [d], Joon-Hak Lee [a], Sean S. Lee [a, **], Byong-Hun Jeon [a, *]

[a] Department of Earth Resources and Environmental Engineering, Hanyang University, 222, Wangsimni-ro, Seongdong-gu, Seoul, 04763, Republic of Korea
[b] School of Environmental Sciences (SES), Jawaharlal Nehru University (JNU), New Delhi, 110067, India
[c] Department of Chemistry & Centre for Bio-Nanotechnology (COBS & H), CCS Haryana Agricultural University, Hisar, 125004, India
[d] Department of Chemistry, College of Science, King Saud University, Riyadh, 11451, Saudi Arabia

HIGHLIGHTS

- Industrial waste sludge was used to develop Al- and Fe-based adsorbents.
- The adsorbents successfully removed arsenate ions from water.
- Angle-resolved-XPS confirmed the retention of As(V) on the adsorbents' surfaces.
- The adsorbents successfully treated As(V) in continuous adsorption mode.
- ABA-packed columns were installed and operated under field conditions.

GRAPHICAL ABSTRACT

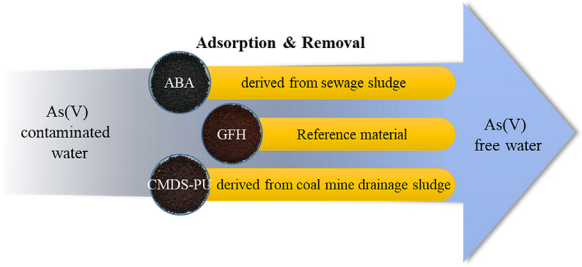

ARTICLE INFO

Article history:
Received 29 June 2019
Received in revised form
5 September 2019
Accepted 9 September 2019
Available online 10 September 2019

Handling Editor: Y. Yeomin Yoon

Keywords:
Arsenate
Granular ferric hydroxide
Aluminum based adsorbent
Coal mine drainage sludge coated polyurethane
Column studies
Empty bed contact time

ABSTRACT

Aqueous arsenate [As(V)] was removed using an aluminum-based adsorbent (ABA) and coal mine drainage sludge coated polyurethane (CMDS-PU) prepared using alum and coal mine sludge, respectively. Their As(V) removal efficiencies were compared with each other and granular ferric hydroxide (GFH). The mineralogy and surface chemistry of materials were determined using wavelength dispersive X-ray fluorescence (WD XRF) and Fourier transform infrared spectroscopy (FTIR), respectively. The angle-resolved X-ray photoelectron spectroscopy (AR-XPS) studies confirmed As(V) retention on the adsorbent surfaces. The adsorption kinetics data were fitted to pseudo second-order rate equation. The faster As(V) uptake kinetics of GFH and ABA (GFH > ABA > CMDS-PU) were attributed to their large pore volume and mesoporous nature. Langmuir adsorption capacities of 22, 31 and 10 mg/g, were achieved for GFH, ABA and CMDS-PU, respectively. As(V) adsorption on GFH, ABA and CMDS-PU was endothermic. GFH and ABA were efficient over a wide pH range (3–10). In column studies, GFH, ABA, and CMDS-PU successfully treated 23625, 842, and 158 bed volumes (BVs) and 2094, 6400, and 17 BVs of As(V)-contaminated water with 9.5 and 27 EBCT, respectively (at pH = 6.0, As_i = 600 μg/L). The GFH and ABA have a potential to be used at large-scale aqueous phase As(V) remediation.

1. Introduction

Arsenic (As) is a well-known carcinogen that exhibits complex chemistry and toxicity, and is considered a priority pollutant (Mandal and Suzuki, 2002; Mohan and Pittman, 2007; Chandra

* Corresponding author.
** Corresponding author.
E-mail addresses: seanlee@hanyang.ac.kr (S.S. Lee), bhjeon@hanyang.ac.kr (B.-H. Jeon).
[1] These authors contributed equally.

https://doi.org/10.1016/j.chemosphere.2019.124832
0045-6535/

et al., 2010). The arsenic presence in drinking water has been reported in Argentina, Chile, China, Mongolia, Taiwan, Nepal, Japan, Mexico, Poland, Vietnam, and the USA (Banerji et al., 2019; Kumar et al., 2019). Both anthropogenic and geogenic sources contribute to arsenic in water (Kumar et al., 2019). Arsenic enters the groundwater through the oxidation of As-bearing sulfide minerals, the reduction of As-rich ferric oxyhydroxides and aluminum-hydroxides, and the ion exchange of adsorbed As, mainly with anions such as phosphate, bicarbonate and silicate (Nickson et al., 2000; McArthur et al., 2001). Geothermally heated water may liberate As from surrounding rocks (Sarkar and Paul, 2016). In the vicinity of mines, As may contaminate soil and water due to the oxidation of As-bearing sulfide ores (McCarty et al., 2011). South Korea is facing groundwater arsenic contamination due to abandoned mining areas in which thousands of metal mines were operated in the early 20th century (McCarty et al., 2011).

In general, organometallic compounds of metals such as tin, mercury, and lead, particularly methylated species, are more harmful than their inorganic species. However, inorganic As is more toxic than its organic forms (Singh et al., 2011; Sarkar and Paul, 2016). Arsenic is mainly responsible for skin cancer (Singh et al., 2011). In view of its toxicity, the prescribed limit of inorganic As in drinking water was reduced by the World Health Organization (WHO) and the United States Environmental Protection Agency (USEPA) from 50 to 10 μg/L (McCarty et al., 2011). The As limit in drinking water has been further reduced in some states of the USA (5 μg/L: New Jersey and South Carolina) and in Australia (7 μg/L) (Chakraborti, 2016). Unfortunately, many developing countries in Asia (India, Bangladesh, Sri Lanka) and Latin America (Argentina, Bolivia, Peru) (Kumar et al., 2019) still use 50 μg/L as a permissible level of As in drinking water.

Physicochemical methods including coagulation, precipitation, ion exchange, reverse osmosis (RO), and adsorption have been used for aqueous phase As remediation. These methods generally suffer from issues such as sludge management, high cost and tedious implementation (Mondal et al., 2006; Choong et al., 2007; Mohan and Pittman, 2007; Malik et al., 2009; Sharma and Sohn, 2009; Kumar et al., 2019). Among the various methods, adsorption, is particularly attractive for aqueous phase As removal (Cho et al., 2016; Kwon et al., 2016). The main challenge in adsorption methods is the selection of an efficient, disposable, and cost-effective material. Performance comparison of new adsorbents is very time-consuming and costly. Iron and aluminum-based adsorbents might be suitable for this purpose due to their relatively high surface area, good efficiency, and low cost (Goldberg and Johnston, 2001; Dou et al., 2013; Lekić et al., 2013; Chen et al., 2014). The development of effective adsorbents for As(V) treatment in point of entry (POE) and point of use (POU) water treatment systems has been investigated in a number of studies. Such adsorbents should not require hazardous desorption agents, and should allow for easy maintenance of the adsorption system (MDE, 2004).

In view of the above, this study evaluated aluminum- and iron-based adsorbents for aqueous As(V) remediation. The iron-based adsorbent was derived from coal mine drainage sludge, a byproduct of coal mine drainage treatment (South Korea). The sludge was coated with polyurethane (CMDS-PU) and used for As(V) remediation. Similarly, an aluminum-based adsorbent (ABA) was prepared using alum sludge produced by wastewater or sewage treatment processes (South Korea). Adsorbents were characterized using FTIR, WDXRF, AR-XPS. Batch operational parameters including contact time, temperature, solution pH, and As(V) concentration, were optimized. The As(V) removal performances of ABA and CMDS-PU were compared with that of granular ferric hydroxide (GFH). Furthermore, fixed-bed design parameters were also evaluated.

2. Experimental

2.1. Materials and methods

All the reagents used in the investigation were of analytical reagent (A.R.) grade unless otherwise specified. As(V) stock solution was prepared using sodium arsenate dibasic hepta-hydrate ($Na_2HAsO_4{\cdot}7H_2O$: Sigma-Aldrich, USA). Hydrochloric acid (0.1 M) (HCl: Sigma-Aldrich, USA) and sodium hydroxide (0.1 M) (NaOH: Sigma-Aldrich, USA) were used to adjust the pH of solutions, which was measured using a microprocessor based digital pH meter (Thermo Scientific, Orion Star A215, USA). Deionized (D.I) water (Millipore, USA) was used in all the batch and column experiments.

Aluminum based adsorbent (ABA, Patent No. 10–1344235, Patent holders: Chonbuk National University and Dasan Consultant Corporation, Republic of Korea) and coal mine drainage sludge coated with polyurethane (received from Korea University and Beautiful Environmental Construction Corporation, Republic of Korea) were used in this study. Briefly, sludge samples were collected and oven dried at 105 °C for 24h. The samples were ground and sieved to 150 μm particle size. The adsorption potentials of two sludge-based materials were compared with that of commercially available granular ferric hydroxide (GFH: GEH 120, LENNTECH, Germany).

2.2. Characterization

The chemical composition of the adsorbent samples was determined using wavelength dispersive X-ray fluorescence (WD XRF: ZSX Primus IV, Rigaku, Japan). Fourier transform infrared spectroscopy (FTIR: Nicolet iS50, Thermo Fisher Scientific, U.K.) in the range of 400–4000 cm^{-1} was used to examine the surface groups present on the adsorbent samples. An angle-resolved X-ray photoelectron spectrometer (AR-XPS: Theta Probe ARXPS, Thermo Fisher Scientific, U.K.), equipped with an MXR1 Gun (400 μm, 15 keV), high resolution electron analyzer (on Ag3d5/2 peak: ≤ 0.5 eV FWHM), and energy source (monochromated Al-Kα (1486.6 eV)) was used to study the retention of As(V) on the adsorbent surfaces. A Brunauer–Emmett–Teller (BET) surface area analyzer (BET Micrometrics, ASAP 2020 V3.04 H) was used to determine the surface area of adsorbents. The solid addition method (Oladoja and Aliu, 2009) was used to determine the point of zero charge (pH_{PZC}) of adsorbent samples.

2.3. Adsorption studies

2.3.1. Batch studies

The As(V) adsorption experiments were carried out in 50 mL vial. A 20 mL aliquot of As(V) solution was equilibrated with a 0.02 g adsorbent for 7 days on a water bath shaker incubator at 250 rpm. Subsequently, the solid and solution phases were separated using membrane filtration (0.45 μm). The residual As(V) concentration was analyzed using inductively couple plasma-optical emission spectrometry (ICP-OES: Optima 3000DV, PerkinElmer, USA). The amount of As(V) adsorbed on the adsorbent samples was evaluated using the equations (1) and (2).

$$Adsorption(\%) = \frac{C_i - C_e}{C_i} \times 100 \quad (1)$$

$$Adsorption\ capacity(q_e, mg/g) = (C_i - C_e) \times \frac{V}{m} \quad (2)$$

where C_i and C_e are the initial and equilibrium As(V) concentrations, respectively, V is the adsorbate volume, and m is the

adsorbent mass. All the experiments were carried out in duplicate, and the mean values are reported. The relative standard deviation (RSD) was less than 10%, which was considered acceptable (Lindberg et al., 2004). Blank experiments were also run to avoid any detectable As(V) adsorbed on the walls of the glassware.

Effect of pH on As(V) adsorption was carried out in the range 3.0–10.0. Effect of contact time on As(V) adsorption (C_i: 30 mg/L; pH: 6.0 ± 0.1) was carried out for up to 72 h. As(V) adsorption equilibrium studies were studied at 10 and 25 °C. Effect of concentration on As(V) adsorption was studied in the range 1–100 mg/L.

2.3.2. Column studies

Information obtained from breakthrough tests is required in designing a pilot scale column. Therefore, column studies were carried out in an acryl column (Fig. S1). A peristaltic pump (RP-MH, Furue Science, Japan) was used in upflow mode to pump 600 μg/L of As(V) solution through the column. To assess the potential of the adsorbents for As(V) removal from water, the empty bed contact time (EBCT) and flow rate were 9.5 or 27 min and 1 mL/min, respectively. As(V) breakthrough was defined as 50 μg/L (Maximum Contaminant Level, MCL).

3. Results and discussion

3.1. Characterization of the adsorbent

Photographs of the three adsorbents, GFH (reddish), ABA (brown), and CMDS-PU (grayish white), are shown in Fig. S2. Adsorbent granules were 1–2 mm in diameter. The morphological parameters are summarized in Table 1. The specific surface area (SSA) was determined using BET method. The SSAs of powdered GFH, ABA, and CMDS-PU were 222, 102, and 4.18 m^2/g. The total pore volume (V_p) of GFH, ABA, and CMDS-PU were 0.28, 0.24, 0.01 cm^3/g, respectively. The micropore (<2.0 nm) surface area was almost negligible in all the cases. The BJH pore volumes were 0.27, 0.23, 0.01 cm^3/g, respectively. The adsorbents average pore width (d_p, 4V/A by BET) were 5.12, 9.40 nm and 13.6 nm for GFH, ABA and CMDS-PU, respectively.

The N_2 adsorption–desorption isotherms and pore size distribution plots of the adsorbents are presented in Fig. S3. Type IV isotherms with an H3 type hysteresis loop were observed for GFH and ABA. This might have been due to capillary condensation in the mesopores (Sing, 1985). The value of the constant C in the BET physisorption model was greater than 1 (C = 101 and 146 for GFH and ABA, respectively), which further confirmed that GFH and ABA had type IV isotherms. In the case of CMDS-PU, the C value was −85. The pore size distribution mainly demonstrated the presence of mesopores in GFH (2.5–10 nm) and ABA (2.5–50 nm), while CMDS-PU exhibited both mesopores (15–50 nm) and macropores (>50 nm) (Fig. S3). The average pore size (d_p) of 2–50 nm is characteristic of mesoporous materials, and is in accordance with a type IV isotherm. CMDS-PU was partially mesoporous, but its relatively low pore volume (V_p) of 0.01 cm^3/g may limit its adsorption capacity. Raw laterite, in spite of containing high amount of Fe and Al, has been reported to be less effective in As(V) adsorption due to its low porosity and low SSA (Maiti et al., 2010). GFH and ABA have similar porosities. CMDS-PU is a low-porosity material versus GFH and ABA (Fig. S3 and Table 1), with properties more similar to those of laterite (SSA = 181 ± 4 m^2/g, V_p = 0.35 ± 0.01 mL/g) (Maiti et al., 2010).

The physicochemical properties of granular adsorbents are summarized in Table 2. The iron content of GFH, being a ferric based medium, was relatively higher (56.0%) than ABA (4.47%) and CMDS-PU (28.7%). ABA was characterized by aluminum (16.0%) silica (19.2%) and oxygen (51.0%). The pH_{PZC} values of GFH, ABA, CMDS-PU were 5.2, 5.0, 9.2, respectively (Table 2).

Table 2
Physicochemical properties of GFH, ABA, CMDS-PU.

Element (wt.%)[a]	GFH	ABA	CMDS-PU
Al	ND	16.0	ND
Ca	ND	ND	2.44
Fe	56.0	4.47	28.7
K	ND	1.94	ND
Mg	ND	1.01	0.45
Mn	0.12	ND	0.47
Si	0.09	19.2	1.78
O	38.3	51.0	50.3
Cl	3.27	ND	ND
C	1.71	3.37	15.6
pH_{PZC}	5.2	5.0	9.2
Packing density (g/cm)	1.361	0.691	0.326

[e]Elemental composition was estimated through wavelength dispersive x-ray fluorescence (WD XRF) analysis. ND: Not detectable.

Table 1
Surface area, pore volume, and pore size of the adsorbents.

Characteristic	GFH	ABA	CMDS-PU
Surface area (m^2/g)			
Single point surface area	215.78 (at P/Po = 0.195)	99.72 (at P/Po = 0.199)	4.10 (at P/Po = 0.219)
BET surface area:	222	102	4.18
Langmuir surface area:	286	132	5.37
[a]BJH adsorption cumulative surface area of pores (1.70–300 nm diameter)	250	98.2	1.57
[a]BJH desorption cumulative surface area of pores (1.7000–300.0000 nm diameter)	277	176	2.98
Pore volume (cm^3/g)			
Single point adsorption total pore volume of pores	0.28 (at P/Po = 0.99, diameter < 356.1 nm)	0.24 (at P/Po = 0.98, diameter <182.5 nm)	0.01 (at P/Po = 0.99, diameter < 325.9 nm)
[a]BJH adsorption cumulative volume of pores (1.70–300.00 nm diameter)	0.27	0.23	0.01
[a]BJH desorption cumulative volume of pores (1.70–300.00 nm diameter)	0.28	0.24	0.01
Pore size (nm)			
Adsorption average pore width (4V/A by BET):	5.12	9.40	13.6
[a]BJH adsorption average pore diameter (4V/A):	4.44	9.54	33.0
[a]BJH desorption average pore diameter (4V/A):	4.08	5.51	19.2

[a] BET= Brunauer-Emmett-Teller (this method is used to estimate the surface area based on multilayer adsorption on a non-porous solid), BJH = Barrett-Joyner-Halenda (this method is used to determine pore size distribution of a mesoporous solid).

Infrared (IR) studies of pristine and As(V)-loaded adsorbents were performed, and the results are illustrated in Fig. 1. The presence of hydroxyl groups (OH) on the GFH, ABA and CMDS-PU surfaces was confirmed by OH stretching band between 3000 and 3500 cm^{-1} (Parga et al., 2009). Additionally, the peak between 1572 and 1813 cm^{-1} (at ~1640), for all three adsorbents was due to hydroxyl bending, γ′(OH) water bending and overtones (Parga et al., 2009). The band at ~1090 cm^{-1} in ABA spectrum was attributed to the formation of hydroxo complexes (-FeOH, -Fe−OH−Fe) of metal hydroxides (Devi et al., 2014). The CMDS-PU spectrum contained many complicated absorption peaks in the fingerprint region (1500−500 cm^{-1}), mainly due to different bending vibrations within the molecule. This is characteristics of aromatic compound, polyurethane in the case of CMDS-PU(Fig. S4). The characteristic absorption peaks between 3430 and 3300 cm^{-1} in CMDS-PU were attributed to the stretching vibration of the free O−H and N−H of hydrogen bonded amino group, those at 2970−2840 cm^{-1} to CH_2 and CH_3 stretching vibration, those at 1720−1600 cm^{-1} to C═O stretching of the bonded carbonyl, those at 1400−1305 cm^{-1} to C−N, and those at 1100−1000 cm^{-1} to −C−O−C. These peaks confirmed the presence of urethane on CMDS-PU surface. The absorption due to −NCO was observed between 2300 and 2200 cm^{-1} (Olorundare et al., 2015). The adsorption of As(V) did not induce any significant changes in the IR spectra except that slight change in peak intensity and peak positions. This suggested that the surface chemistry of the adsorbents played an insignificant role in determining their As(V) retention.

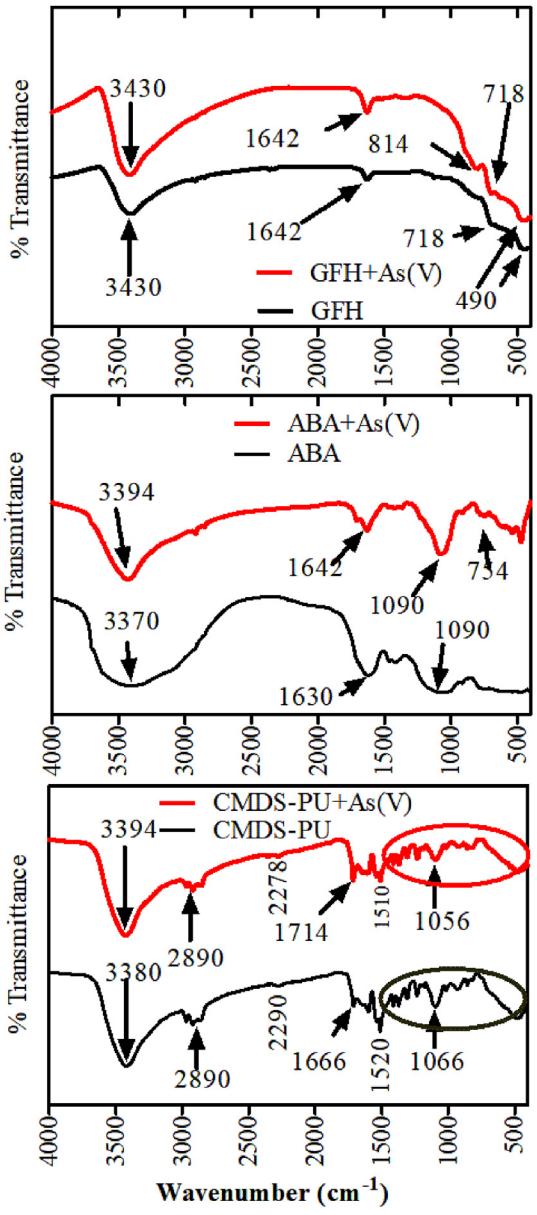

Fig. 1. Fourier transform infrared (FTIR) spectra of pristine and As(V)-loaded adsorbents.

The wide-scan AR-XPS spectra of pristine (GFH, ABA, CMDS-PU) and As(V)-loaded (GFH-As, ABA-As, CMDS-PU-As) adsorbents are depicted in Fig. 2. Major peaks at binding energies of 248.6 (C1s), 711.1 (Fe2p3), 400.81 (N1s), 530.4 (O1s), and 100.4 (Si2p) eV were observed for GFH. In ABA, in addition to peaks at 284.6 (C1s), 711.2 (Fe2p3), 399.9 (N1s), 351.9 (O1s), and 102.3 (Si2p), a peak at 73.7 eV corresponding to Al2p3 indicated the presence of aluminum in ABA (Fig. 2). The peaks in the AR-XPS wide scan spectra for CMDS-PU at 248.6 (C1s), 710.6 (Fe2p3), 399.4 (N1s), 530.0 (O1s) and 101.0 eV (Si2p) were similar to those observed for GFH. The appearance of a peak corresponding to As2p3 at ~1327 eV for GFH-As, ABA-As, CMDS-PU-As was the most significant change in the spectra, and confirmed the presence of As(V) on all three adsorbent surfaces after As(V) adsorption (Fig. S5, Table S1).

3.2. Kinetics of As(V) adsorption onto GFH, ABA, and CMDS-PU

The parameters obtained from kinetics study plots (Fig. 3) are necessary for the design of appropriate sorption units. The different As(V) adsorption kinetics among the adsorbents could be attributed to the different physicochemical characteristics (surface area, porosity, pH_{PZC}, mineralogy and surface chemistry) of the materials. The As(V) uptake rate was initially rapid due to the availability of a large number of adsorption sites on the adsorbents. Typically, 50% of the total adsorption in terms of their respective capacities (q_t) completed in 20 h (GFH), 10 h (ABA), and 20 h (CMDS-PU) (Fig. 3), after which the kinetics slowed down until equilibrium was reached. Equilibrium was attained in 100, 50 and 200 h for GFH, ABA and CMDS-PU, respectively.

Pseudo-first-order (PFO) and pseudo-second-order (PSO) equations were used to fit experimental results. The rate constants are tabulated in Table 3. Pseudo-second-order (PSO) rate equation better fitted the As(V) adsorption data obtained for all the three adsorbents. This indicate that As(V) adsorption occurred on the active sites of the solid phases via chemisorption (Dou et al., 2013). PSO model has been proven to be superior to the PFO model for fitting of As(V) adsorption data (Dou et al., 2013; Ryu et al., 2017). The PFO/PSO equations describe kinetics data as a generalized removal process with one rate-controlling step. However, the intraparticle diffusion (IPD) model provides a more comprehensive view of adsorption as a series of distinct steps (D'Arcy et al., 2011; Dou et al., 2013). The multilinearities observed over the entire time range for this model (Fig. 3) indicated that the adsorption process was governed by two or more steps rather than only one. The first linear portion (or, in case of GFH, the two initial portions) of the plot of q_t verses $t^{1/2}$ had a steeper slope, indicating the external diffusion of As(V) from the bulk to the exterior surface of adsorbent was the rate limiting step at this stage. The second linear portion with a shallower slope represented a stage in which IPD was the rate limiting step; diffusion into the mesopores/micropores dominated during this stage (Cheung et al., 2007).

Theoretical treatments of IPD are based on Fick's first law of diffusion (McKay et al., 1987). An increase in the adsorbate concentration acts as the driving force, leading to rapid adsorption reaction. The rate parameter (k_p) followed the order

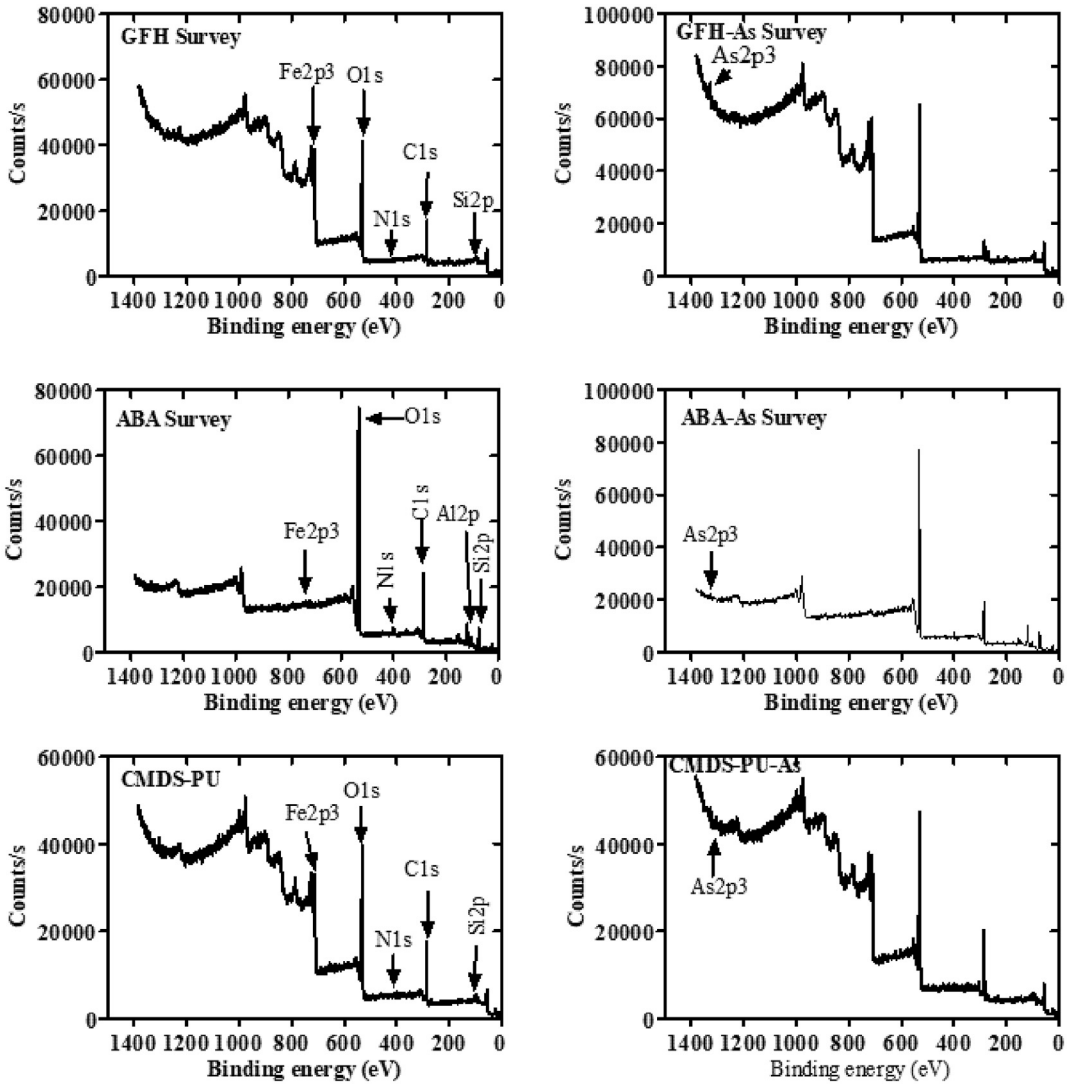

Fig. 2. Angle-resolved X-ray photoelectron spectroscopy (AR-XPS) wide scan spectra of the pristine (left side) and As(V)-loaded (right side) adsorbents.

GFH > ABA > CMDS-PU, which was same as their adsorption capacity order (Table 3). The rate parameters were positively correlated with the pore volumes and interparticle porosities of adsorbents (Table 1). The rapid As(V) adsorption kinetics on GFH and ABA were attributed to their large pore volumes and interparticle porosities compared to those of CMDS-PU granules. The q_t verses $t^{0.5}$ plots were neither linear nor pass through the origin (Fig. 3), except for initial stages of GFH and CMDS-PU; therefore, intra-particle diffusion was not the rate-controlling step. The plot showed multi-linearity, indicating a complex adsorption process (Singh et al., 2012).

3.3. Effect of pH on As(V) adsorption

The pH of a system is a master variable in environmental studies, influencing both the surface chemistry of the adsorbent and the speciation of the adsorbate. Specifically, As(V) can exist in solution as H_3AsO_4, $H_2AsO_4^-$, ($pK_a^1 = 2.3$), $HAsO_4^{2-}$ ($pK_a^2 = 6.8$), and AsO_4^{3-} ($pK_a^3 = 11.6$) (Goldberg and Johnston, 2001; Mohan and Pittman, 2007). Therefore, the adsorption of As(V) onto GFH, ABA, and CMDS-PU was quantitatively estimated in the pH range of 3–10 (Fig. 4). In the case of GFH, the As(V) adsorption decreased slowly with increasing solution pH up to pH 5, then decreased relatively rapidly above this value. This behavior is typical of the adsorption of As(V) onto most iron (hydr)oxides (Maiti et al., 2012). For ABA, the As(V) adsorption decreased regularly up to pH 10. The CMDS-PU granules showed a significant adsorption drop when pH was increased from pH 3.0 to 6.0, followed by a plateau from pH 6 to pH 8 then an adsorption decreases from pH 8 to 10. No apparent correlation was observed between the pH_{PZC} value and adsorption capacity (q) of the materials with varying pH values.

The decrease in As(V) removal efficiency with increasing pH may be due to the unfavorable adsorption conditions such as repulsion between anionic species in basic systems. Solution pH values of <6.0 favor the protonation of the oxides surface ($= Fe - OH_2^+$), which increases the electrostatic attraction between the surface and the negatively charged arsenic species ($H_2AsO_4^-$), leading to adsorption enhancement. At pH > 7.2, the repulsion between the negatively charged = Fe–O- surface and $HAsO_4^{2-}$ and AsO_4^{3-} decreased the As(V) removal. The pH effect and the role of electrostatic interactions will be minimal at low initial As(V) concentration due to availability of abundant surface sites.

This adsorption behavior of iron (hydr)oxide media and other minerals towards As(V) as a function of the pH has been reported in

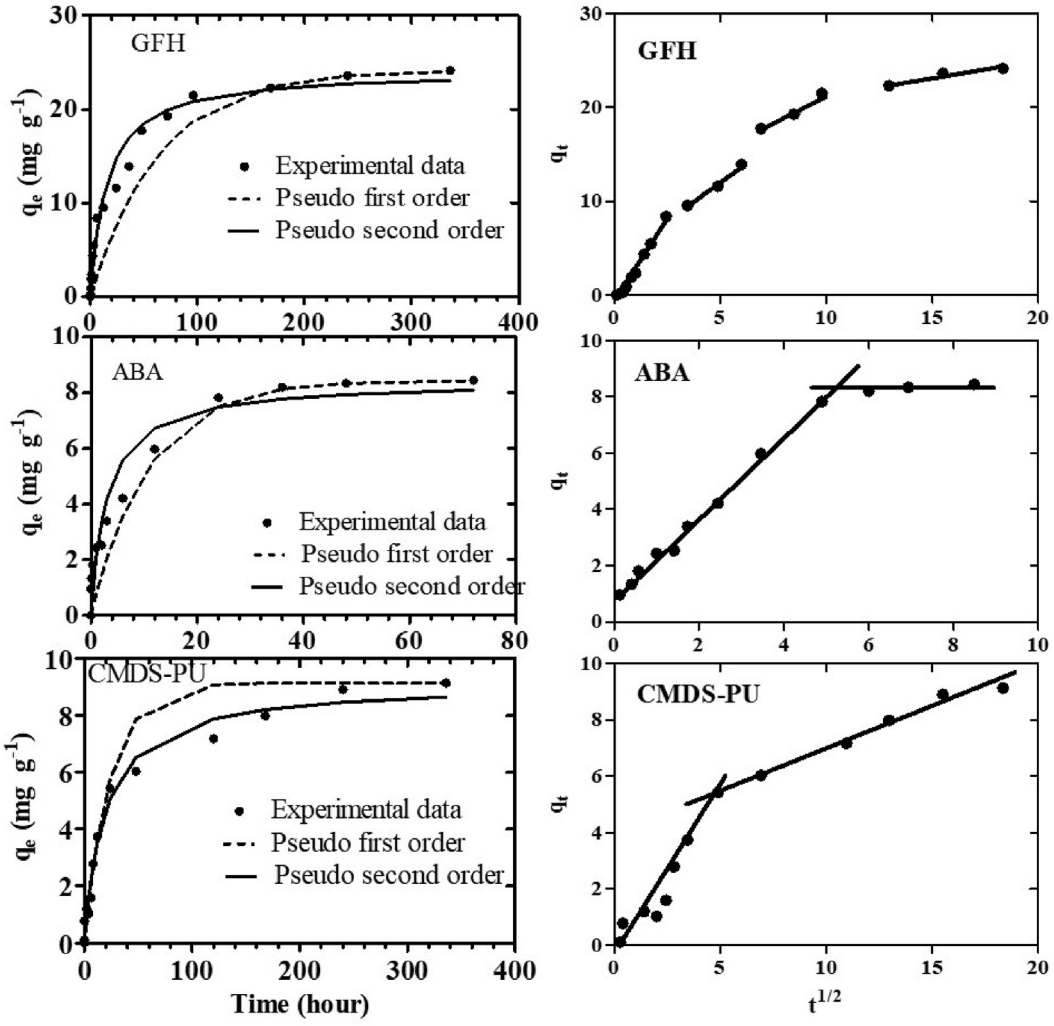

Fig. 3. As(V) adsorption kinetics on granular ferric hydroxide (GFH), aluminum-based adsorbent (ABA), and coalmine drainage sludge coated polyurethane (CMDS-PU) and fitting of kinetic data to pseudo-first order, pseudo-second order, and intraparticle diffusion models(Initial As(V) concentrations: 30 mg/L; adsorbent dose: 1.0 g/L; pH: 6.0 ± 0.1; shaking speed: 150 rpm; temperature: 25 ± 1 °C).

Table 3
Kinetic parameters for As(V) adsorption on GFH, ABA, CMDS-PU.

Kinetic models	Parameter	GFH	ABA	CMDS-PU
Pseudo-first-order (PFO)[a]	q_{cal} (mg/g)	24.0	8.43	9.14
	q_{exp} (mg/g)	24.2	8.44	9.14
	k_1(1/h)	0.016	0.091	0.014
	R^2	**0.959**	**0.993**	**0.954**
	RMSE	3.35	0.98	1.28
Pseudo second-order (PSO)[b]	q_{cal} (mg/g)	23.1	8.10	8.65
	q_{exp} (mg/g)	24.2	8.44	9.14
	k_2(g/(mg·h))	0.003	0.039	0.005
	R^2	**0.996**	**0.993**	**0.987**
	RMSE	1.43	0.77	0.53
	$h(k_2 \times q_{cal}^2)$	1.60	2.56	0.37
Intra-particle diffusion (IPD)[c]	k_p	1.51	1.07	0.56
	R^2	**0.893**	**0.924**	**0.909**
	RMSE	5.85	1.33	3.00

h = initial rate of reaction; q_{cal} = calculated adsorption capacity; q_{exp} = experimentally determined adsorption capacities; RMSE = root mean square error (sy·x). (Experimental conditions: $As(V)_i$ = 30 mg/L, pH = 6 ± 0.1, dose = 1.0 g/L, at 25 °C).

[a] Langergren's pseudo-first-order (PFO) equation, $q_t = q_e(1\text{-}e^{-k1t})$.

[b] Ho's pseudo-second-order (PSO) equation, $q_t = q_e^2 k_2 t/(1+q_e k_2 t)$.

[c] Intra-particle diffusion model equation, $q_t = k_p t^{1/2} + C$.

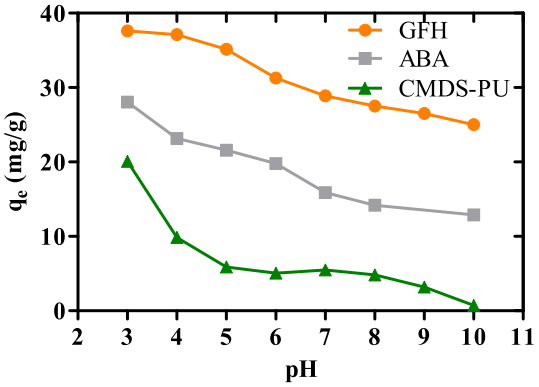

Fig. 4. Effect of the solution pH on As(V)adsorption on granular ferric hydroxide (GFH), aluminum-based adsorbent (ABA), coalmine drainage sludge coated polyurethane (CMDS-PU)[As(V): 40 mg/L; dose: 1.0 g/L; temperature: 25 ± 1 °C].

previous studies (Möller and Sylvester, 2008; Dou et al., 2013). The electrostatic interaction and ligand exchange mechanisms reported for As(V) adsorption on mineral surface are strongly pH dependent. In particular, the ligand exchange of As(V) with surface $=Fe-OH_2^+$ and Fe–OH groups (iron oxyhydroxide surface) is frequently reported in the literature (Eqns. (3) and (4)) (Möller and Sylvester, 2008; Maiti et al., 2010). Ligand exchange between As(V), surface-coordinated water molecules, and hydroxyl and silicate ions at allophane $(Al_2O_3\cdot(SiO_2)_{1\text{-}2}\cdot(H_2O)_{2\text{-}3})$ has also been observed (Mohan and Pittman, 2007). In contrast to their affinity for As(III), which usually remains relatively constant at typical drinking water pH values (6.5–8.5), their affinity towards As(V) continually decreases as the pH increases.

$$=M-OH + H_2AsO_4^-(\text{As(V) in the pH range 4 – 8}) \rightleftharpoons =MHAsO_4^- + H_2O(M = \text{Fe and Al})) \quad (3)$$

$$=M-OH_2^+ + H_2AsO_4^-(\text{As(V) in the pH range 4 – 8}) \rightleftharpoons =MHAsO_4 + H_3O^+(M = \text{Fe and Al})) \quad (4)$$

3.4. As(V) Adsorption equilibrium studies

Equilibrium adsorption isotherm describe the interactions between solute and adsorbent. Isotherm studies are useful to determine adsorption capacities and other equilibrium isotherm parameters under different conditions. This information is crucial for adsorbent selection and adsorption unit design.

Two parameter Langmuir (Langmuir, 1916, 1917) and Freundlich (1907) isotherm models were employed to fit the sorption equilibrium experimental data (Supplementary Information, SI 1.0). Non-linear modelling using GraphPad Prism (version 5.0 software) was conducted using least square method. The Langmuir isotherm model assumes that adsorption onto the surface takes place in a monolayer fashion, and that adsorption sites are homogeneously distributed on the surface (Langmuir, 1916, 1917). The Freundlich isotherm assumes multilayer adsorption or sorption onto a heterogeneous surface, i.e., a surface with multiple sorption sites with different active energies due to high SSA (Freundlich, 1907). The Freundlich model is valid for adsorption data over a confined range of As(V) equilibrium concentrations (Ce). The adsorption parameters obtained from the isotherm model studies are given in Table 4. The Langmuir model better fitted the data (R^2: GFH = 0.998, ABA = 0.936, CMDS-PU = 0.976) versus Freundlich model (R^2: GFH = 0.664, ABA = 0.769, CMDS-PU = 0.958), indicating that As(V)

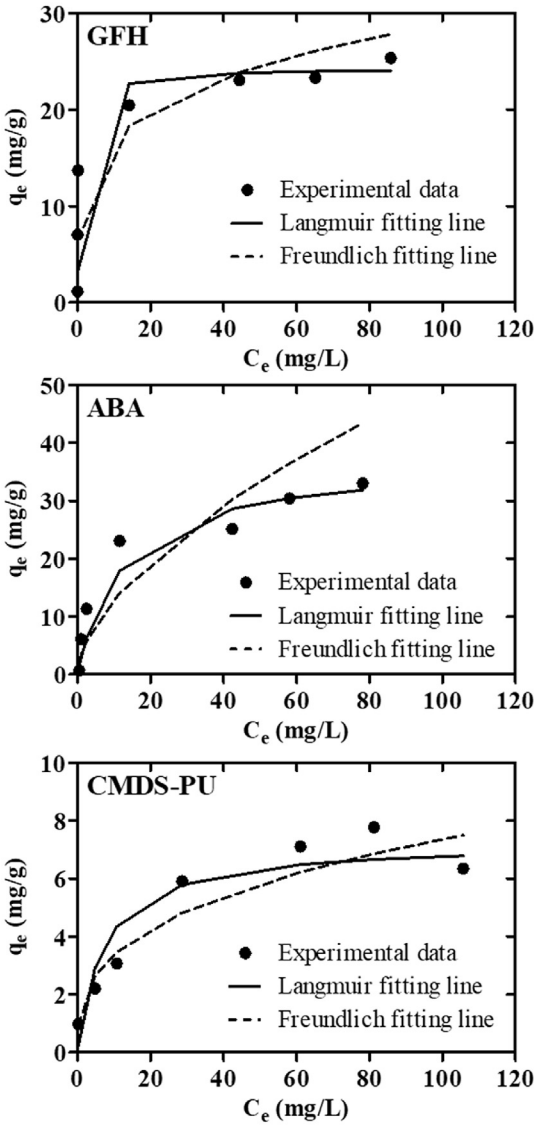

Fig. 5. Isotherms and modelling results for the adsorption of As(V) on granular ferric hydroxide (GFH), aluminum-based adsorbent (ABA), and coal mine drainage sludge coated polyurethane (CMDS-PU)(Initial As(V) concentration range: 1–100 mg/L; adsorbent dose: 1.0 g/L; pH: 6.0 ± 0.1; shaking speed: 150 rpm; temperature: 25 ± 1 °C.

Table 4
Langmuir and Freundlich parameters for As(V) adsorption on GFH, ABA, CMDS-PU.

Isotherm model	Parameter	GFH	ABA	CMDS-PU
Two parameter model				
Langmuir[a]	q_{max} (mg/g)	24.36	36.84	7.26
	q_{exp} (mg/g)	24.76	33.02	6.34
	K_L (L/mg)	0.972	0.082	0.138
	R_L	0.009	0.099	0.061
	R^2	**0.998**	**0.936**	**0.976**
	RMSE	4.760	3.337	0.722
Freundlich[b]	K_f (mg/g) (L/mg)$^{1/n}$	9.906	3.312	1.541
	n(1/n)	4.31(0.23)	1.69(0.59)	2.95(0.34)
	R^2	**0.664**	**0.769**	**0.958**
	RMSE	3.633	6.478	0.735

q_{max}, q_{exp} are the Langmuir and experimentally determined adsorption capacities, respectively. RMSE = root mean square error (sy·x).
(Experimental conditions: $As(V)_i$ = 1–100 mg/L, dose = 1.0 g/L, pH = 6 ± 0.1, at 25 °C).
[a] Langmuir model equation, $C_e/q_e = 1/(K_L\cdot q_{max}) + C_e/q_{max}$.
[b] Freundlich model equation, $\log q_e = \log K_f + (1/n)\log C_e$.

adsorption was monolayer in nature. Maximum As(V) adsorption capacities (q_{max}) of 24.4 mg/g (GFH), 36.8 mg/g (ABA), and 7.3 mg/g (CMDS-PU) were obtained (Fig. 5). The Langmuir isotherms were also used to determine the separation factor (R_L) to predict if the adsorption was favorable or unfavorable (Hall et al., 1966; Cho et al., 2016; Kumar et al., 2018) (Supplementary Information, SI 1.1.1). The R_L values lay between 0 and 1, indicating that the adsorption of As(V) on the three adsorbents as favorable (Table 4). The 1/n values obtained for As(V) adsorption onto the adsorbents fell between 0.23 and 0.59, indicating that adsorption was favorable. The adsorption of As(V) on GFH and ABA might be diffusion controlled at low As(V) concentrations while following monomolecular adsorption at high concentrations. The increase in sorption capacity with rise in temperature from 10 to 25 °C demonstrated that the process was endothermic (Fig. S6).

It is difficult to compare different adsorbents used for As(V) remediation due to variation in the experimental conditions and adsorbent characteristics. However, comparative evaluation may provide a brief comparison of the efficiencies of the materials under investigation. The As(V) adsorption capacities of various adsorbents are summarized in Table 5. GFH and ABA showed better As(V) removal capacity than the other adsorbents (Table 5). ABA may therefore has the capacity to be used as a sustainable low-cost adsorbent for As(V) remediation; GFH is commercially available and already used for As removal from water). Even CMDS-PU is superior to several other adsorbents (Table 5).

The values of the constant K_L for the adsorption of As(V) onto GFH, ABA, and CMDS-PU (at 25 °C) are 0.972, 0.082, and 0.138, respectively. The larger the value of K_L, the higher the adsorption energy of GFH, which corresponds to a fast increase in the adsorption rate at lower concentration (Hu et al., 2003; Maiti et al., 2012). The product $q_{max} \cdot K_L$ indicates the relative affinity of the adsorbates towards the adsorbent surfaces (Hu et al., 2003). Therefore, $q_{max} \cdot K_L$ values may be considered for comparative evaluation in place of q_{max} alone. The $q_{max} \cdot K_L$ values for different adsorbents are reported in Table 5. It is clear that GFH and ABA have higher adsorption affinity than many adsorbents used for As(V) at low equilibrium As(V) concentrations.

3.5. Column studies

Column studies were used to examine the ability of the adsorbents to remove As(V) from contaminated water. Breakthrough occurred after 23625 (GFH), 842 (ABA) and 158 (CMDS-PU) bed volumes (BVs) (EBCT = 9.5, pH = 6.0) and 2094 (GFH), 6400 (ABA) and 17 (CMDS-PU) bed volumes (EBCT = 27, pH = 6.0) when As(V) contaminated water was passed through GFH, ABA, and CMDS-PU granules packed columns, respectively (Fig. 6). GFH maintained below MCL after one breakthrough. The CMDS-PU adsorbent exhibited the lowest efficiency, which was attributed to its dense and compact surface, small pore size, small pore volume, and low porosity. The better kinetics and adsorption efficiencies of GFH and ABA in both the batch tests and column experiments were due to their higher specific surface areas and porosities. Following the column studies, a small-scale As(V) remediation experiment was successfully applied at the field level (Fig. S7).

4. Conclusion

A low-cost aluminum-based adsorbent (ABA), coal mine drainage sludge coated with polyurethane (CMDS-PU), and granular ferric hydroxide (GFH) were characterized and used in aqueous As(V) remediation. The GFH and ABA granules were mesoporous, which favored As(V) adsorption. Arsenate was successfully removed using GFH and ABA. As(V) adsorption using CMDS-PU was unfavorable. The adsorption process was endothermic. The As(V) adsorption kinetics onto GFH, ABA and CMDS-PU followed a pseudo-second order rate equation. Application of the intraparticle

Table 5
Comparison of As(V) adsorption efficiencies of adsorbents used in this study with those previously reported other adsorbents.

Adsorbent	pH_i	Temp (K)	Dose (g/L)	Conc.(mg/L)	q_{max} (mg/g)	K_L (L/mg)	$K_L \cdot q_{max}$	Reference
Mn oxide loaded sand	4.5	298	2.00	1–100	0.09	1.02	0.10	Chang et al. (2009)
Iron sand	4.5	298	2.00	1–100	0.12	2.16	0.26	Chang et al. (2009)
Fe-oxide loaded sand	4.5	298	2.00	1–100	0.22	0.61	0.13	Chang et al. (2009)
Magnetite	7.5	298[b]	5.0	–	0.25	0.424	0.11	Giménez et al. (2007)
Goethite	6.5	298[b]	5.0	–	0.45	1.86	0.84	Giménez et al. (2007)
Raw laterite	5.5	302	20.0	0.20–20	0.51	2.78	1.41	Maiti et al. (2008)
Laterite iron concretions	7.0	295	5.00	0.10–2.0	0.71	0.264	0.19	Partey et al. (2008)
IMOCS (industrial byroducts)	7.0	298	10	–	0.77	1.18	0.91	Lekić et al. (2013)
Hematite	7.3	298[b]	5.0	–	0.83	0.0066	0.01	Giménez et al. (2007)
GFH (commercial sorbents)	7.0	298	10	–	1.17	2.21	2.59	Lekić et al. (2013)
Fe-coated pottery	7.0	298	–	–	1.74	39.3	68.4	Dong et al. (2009)
HIER (commercial sorbents)	7.0	298	10	–	2.52	19.7	49.6	Lekić et al. (2013)
MBFS (industrial byproducts)	7.0	298	10	–	2.79	18.6	51.9	Lekić et al. (2013)
BFS	7.0	298	10	–	4.04	12.7	51.3	Lekić et al. (2013)
Fe_3O_4–RGO(M2)	7.0	293	0.2	3.0–7.0	5.83	0.42	2.44	Chandra et al. (2010)
Fe_3O_4–RGO(M1)	7.0	293	0.2	3.0–7.0	5.27	0.40	2.11	Chandra et al. (2010)
Fe_2O_3–OMC-500 °C	–	298	1.0	0.2–30	8.00	1.08	8.64	Wu et al. (2012)
Ce–Fe oxide@cCNTs-A[a]	7.5	298	0.20	1.0–20	16.8	0.63	10.6	Chen et al. (2013)
Fe_2O_3–OMC-300 °C	–	298	1.0	0.2–30	17.9	2.24	40.1	Wu et al. (2012)
Treated laterite	7.0	288	0.50	1.0–5.0	21.6	20.6	445	Maiti et al. (2012)
Treated laterite	7.0	305	0.50	0–0.20	24.1	17.0	409	Maiti et al. (2010)
Ce–Fe oxide@cCNTs[a]	7.5	298	0.20	1.0–20	30.9	2.56	79.1	Chen et al. (2013)
Fe_2O_3–cellulose	7.0	298	1.0	0–25	32.1	0.039	1.25	Yu et al. (2013)
GFH	6.0	298	1.0	1–100	24.3	0.97	23.7	This study
ABA	6.0	298	1.0	1–100	36.8	0.08	3.02	This study
CMDS-PU	6.0	298	1.0	1–100	7.3	0.14	1.00	This study

[a] The decorated CNTs in the absence of NaSDBS are referred to as CF-CNTs-A, and the decorated CNTs in the presence of NaSDBS are referred to as CF-CNTs. Mentions of "room temperature" in the studies were assumed to refer to 25 °C. ABA-aluminum based adsorbent, BFS-blast furnace slag from steel production, CMDS-PU-polyurethane coated coal mine drainage sludge, GFH-granular ferric hydroxide, HIER-hybrid ion exchange resin coated with nano scale iron oxide particles. IMOCS-iron-manganese oxide coated sand, OMC- ordered mesoporous carbon, RGO-reduced graphene oxide.

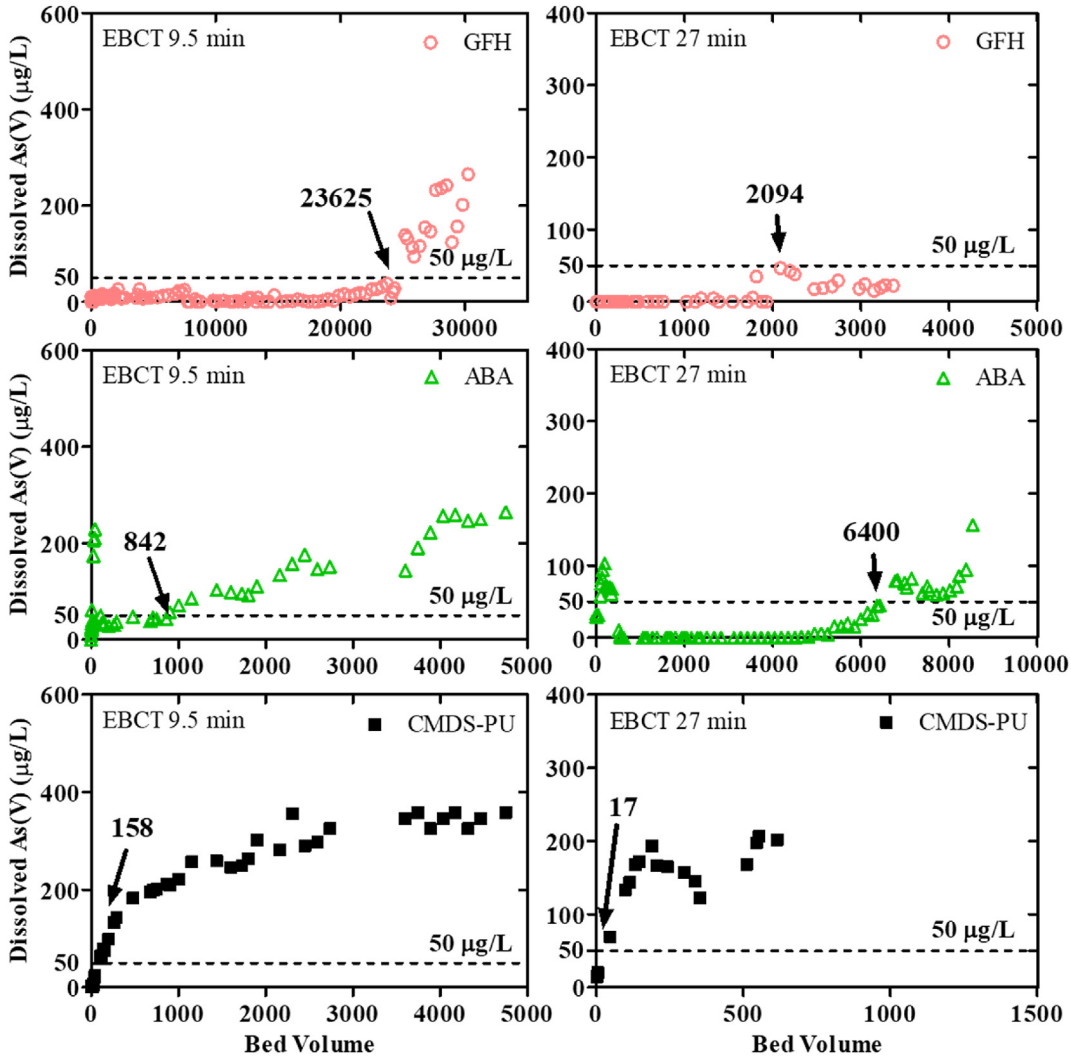

Fig. 6. As(V) adsorption breakthrough curves obtained for granular ferric hydroxide (GFH), aluminum-based adsorbent (ABA), and coalmine drainage sludge coated polyurethane (CMDS-PU) (Initial As(V) concentration: 600 µg/L; pH: 6.0; EBCT: 9.5 and 27 min).

diffusion model revealed the adsorption process to be complex. High pH negatively influenced the adsorption capacity of GFH, ABA, and CMDS-PU. Evaluation of the efficiencies of the adsorbents in a column demonstrated that 23625 (GFH), 842 (ABA) and 158 (CMDS-PU) bed volumes (BVs) (for EBCT = 9.5, at pH = 6.0) and 2094 (GFH), 6400 (ABA) and 17 (CMDS-PU) BVs (EBCT = 27, at pH = 6.0) of As(V)-contaminated water could be treated with columns packed with GFH, ABA, and CMDS-PU, respectively, before breakthrough occurred (50 µg/L). The ABA-packed columns were successfully installed and operated under field conditions (near mining area) in South Korea. Such materials might be used for As remediation in Latin America, certain areas of India, Bangladesh and South Korea.

Acknowledgements

This study was supported by Korea Institute of Energy Technology Evaluation and Planning grants funded by the Ministry of Trade, Industry and Energy of the South Korean government (No. 20182510102420).

Appendix A. Supplementary data

Supplementary data to this article can be found online at https://doi.org/10.1016/j.chemosphere.2019.124832.

References

Banerji, T., Kalawapudi, K., Salana, S., Vijay, R., 2019. Review of processes controlling Arsenic retention and release in soils and sediments of Bengal basin and suitable iron based technologies for its removal. Groundwater for Sustainable Development 8, 358–367.
Chakraborti, D., 2016. Is WHO guideline value of arsenic in drinking water 10 ppb in the developing countries safe to drink? BLDE University Journal of Health Sciences 1, 57.
Chandra, V., Park, J., Chun, Y., Lee, J.W., Hwang, I.-C., Kim, K.S., 2010. Water-dispersible magnetite-reduced graphene oxide composites for arsenic removal. ACS Nano 4, 3979–3986.
Chang, Y.-Y., Lee, S.-M., Yang, J.-K., 2009. Removal of as (III) and as (V) by natural and synthetic metal oxides. Colloid. Surf. Physicochem. Eng. Asp. 346, 202–207.
Chen, B., Zhu, Z., Ma, J., Qiu, Y., Chen, J., 2013. Surfactant assisted Ce–Fe mixed oxide decorated multiwalled carbon nanotubes and their arsenic adsorption performance. J. Mater. Chem. 1, 11355–11367.
Chen, L., Xin, H., Fang, Y., Zhang, C., Zhang, F., Cao, X., Zhang, C., Li, X., 2014. Application of metal oxide heterostructures in arsenic removal from contaminated water. J. Nanomater. 2, 2014.
Cheung, W., Szeto, Y., McKay, G., 2007. Intraparticle diffusion processes during acid dye adsorption onto chitosan. Bioresour. Technol. 98, 2897–2904.
Cho, D.-W., Jeon, B.-H., Jeong, Y., Nam, I.-H., Choi, U.-K., Kumar, R., Song, H., 2016.

Synthesis of hydrous zirconium oxide-impregnated chitosan beads and their application for removal of fluoride and lead. Appl. Surf. Sci. 372, 13–19.
Choong, T.S., Chuah, T., Robiah, Y., Koay, F.G., Azni, I., 2007. Arsenic toxicity, health hazards and removal techniques from water: an overview. Desalination 217, 139–166.
D'Arcy, M., Weiss, D., Bluck, M., Vilar, R., 2011. Adsorption kinetics, capacity and mechanism of arsenate and phosphate on a bifunctional TiO2–Fe2O3 bi-composite. J. Colloid Interface Sci. 364, 205–212.
Devi, R.R., Umlong, I.M., Das, B., Borah, K., Thakur, A.J., Raul, P.K., Banerjee, S., Singh, L., 2014. Removal of iron and arsenic (III) from drinking water using iron oxide-coated sand and limestone. Applied Water Science 4, 175–182.
Dong, L., Zinin, P.V., Cowen, J.P., Ming, L.C., 2009. Iron coated pottery granules for arsenic removal from drinking water. J. Hazard Mater. 168, 626–632.
Dou, X., Mohan, D., Pittman Jr., C.U., 2013. Arsenate adsorption on three types of granular schwertmannite. Water Res. 47, 2938–2948.
Freundlich, H., 1907. Über die adsorption in lösungen. Z. Phys. Chem. 57, 385–470.
Giménez, J., Martinez, M., de Pablo, J., Rovira, M., Duro, L., 2007. Arsenic sorption onto natural hematite, magnetite, and goethite. J. Hazard Mater. 141, 575–580.
Goldberg, S., Johnston, C.T., 2001. Mechanisms of arsenic adsorption on amorphous oxides evaluated using macroscopic measurements, vibrational spectroscopy, and surface complexation modeling. J. Colloid Interface Sci. 234, 204–216.
Hall, K.R., Eagleton, L.C., Acrivos, A., Vermeulen, T., 1966. Pore-and solid-diffusion kinetics in fixed-bed adsorption under constant-pattern conditions. Ind. Eng. Chem. Fundam. 5, 212–223.
Hu, Z., Lei, L., Li, Y., Ni, Y., 2003. Chromium adsorption on high-performance activated carbons from aqueous solution. Separ. Purif. Technol. 31, 13–18.
Kumar, R., Kim, S.-J., Kim, K.-H., Lee, S.-h., Park, H.-S., Jeon, B.-H., 2018. Removal of hazardous hexavalent chromium from aqueous phase using zirconium oxide-immobilized alginate beads. Appl. Geochem. 88, 113–121.
Kumar, R., Patel, M., Singh, P., Bundschuh, J., Pittman Jr., C.U., Trakal, L., Mohan, D., 2019. Emerging technologies for arsenic removal from drinking water in rural and peri-urban areas: methods, experience from, and options for Latin America. Sci. Total Environ. 694.
Kwon, O.-H., Kim, J.-O., Cho, D.-W., Kumar, R., Baek, S.H., Kurade, M.B., Jeon, B.-H., 2016. Adsorption of as (III), as (V) and Cu (II) on zirconium oxide immobilized alginate beads in aqueous phase. Chemosphere 160, 126–133.
Langmuir, I., 1916. The constitution and fundamental properties of solids and liquids. Part I. Solids. J. Am. Chem. Soc. 38, 2221–2295.
Langmuir, I., 1917. The constitution and fundamental properties of solids and liquids. II. Liquids. J. Am. Chem. Soc. 39, 1848–1906.
Lekić, B.M., Marković, D.D., Rajaković-Ognjanović, V.N., Đukić, A.R., Rajaković, L.V., 2013. Arsenic removal from water using industrial by-products. J. Chem., 121024, 2013.
Lindberg, R., Jarnheimer, P.A., Olsen, B., Johansson, M., Tysklind, M., 2004. Determination of antibiotic substances in hospital sewage water using solid phase extraction and liquid chromatography/mass spectrometry and group analogue internal standards. Chemosphere 57, 1479–1488.
Maiti, A., Basu, J.K., De, S., 2010. Development of a treated laterite for arsenic adsorption: effects of treatment parameters. Ind. Eng. Chem. Res. 49, 4873–4886.
Maiti, A., Basu, J.K., De, S., 2012. Experimental and kinetic modeling of as (V) and as (III) adsorption on treated laterite using synthetic and contaminated groundwater: effects of phosphate, silicate and carbonate ions. Chem. Eng. J. 191, 1–12.
Maiti, A., DasGupta, S., Basu, J.K., De, S., 2008. Batch and column study: adsorption of arsenate using untreated laterite as adsorbent. Ind. Eng. Chem. Res. 47, 1620–1629.
Malik, A.H., Khan, Z.M., Mahmood, Q., Nasreen, S., Bhatti, Z.A., 2009. Perspectives of low cost arsenic remediation of drinking water in Pakistan and other countries. J. Hazard Mater. 168, 1–12.
Mandal, B.K., Suzuki, K.T., 2002. Arsenic round the world: a review. Talanta 58, 201–235.
McArthur, J., Ravenscroft, P., Safiulla, S., Thirlwall, M., 2001. Arsenic in groundwater: testing pollution mechanisms for sedimentary aquifers in Bangladesh. Water Resour. Res. 37, 109–117.
McCarty, K.M., Hanh, H.T., Kim, K.-W., 2011. Arsenic geochemistry and human health in South east Asia. Rev. Environ. Health 26, 71–78.
McKay, G., Otterburn, M.S., Aga, J.A., 1987. Intraparticle diffusion process occurring during adsorption of dyestuffs. Water Air Soil Pollut. 36, 381–390.
MDE, 2004. Arsenic Water Treatment for Individual Wells in Maryland. Maryland Department of the Environment Water Management Administration, Maryland.
Mohan, D., Pittman, C.U., 2007. Arsenic removal from water/wastewater using adsorbents—a critical review. J. Hazard Mater. 142, 1–53.
Möller, T., Sylvester, P., 2008. Effect of silica and pH on arsenic uptake by resin/iron oxide hybrid media. Water Res. 42, 1760–1766.
Mondal, P., Majumder, C., Mohanty, B., 2006. Laboratory based approaches for arsenic remediation from contaminated water: recent developments. J. Hazard Mater. 137, 464–479.
Nickson, R., McArthur, J., Ravenscroft, P., Burgess, W., Ahmed, K., 2000. Mechanism of arsenic release to groundwater, Bangladesh and West Bengal. Appl. Geochem. 15, 403–413.
Oladoja, N.A., Aliu, Y.D., 2009. Snail shell as coagulant aid in the alum precipitation of malachite green from aqua system. J. Hazard Mater. 164, 1496–1502.
Olorundare, O., Msagati, T., Krause, R., Okonkwo, J., Mamba, B., 2015. Polyurethane composite adsorbent using solid phase extraction method for preconcentration of metal ion from aqueous solution. Int. J. Environ. Sci. Technol. 12, 2389–2400.
Parga, J., Vazquez, V., Moreno, H., 2009. Thermodynamic studies of the arsenic adsorption on iron species generated by electrocoagulation. Journal of Metallurgy, 286971, 2009.
Partey, F., Norman, D., Ndur, S., Nartey, R., 2008. Arsenic sorption onto laterite iron concretions: temperature effect. J. Colloid Interface Sci. 321, 493–500.
Ryu, S.-R., Jeon, E.-K., Yang, J.-S., Baek, K., 2017. Adsorption of as (III) and as (V) in groundwater by Fe–Mn binary oxide-impregnated granular activated carbon (IMIGAC). Journal of the Taiwan Institute of Chemical Engineers 72, 62–69.
Sarkar, A., Paul, B., 2016. The global menace of arsenic and its conventional remediation-A critical review. Chemosphere 158, 37–49.
Sharma, V.K., Sohn, M., 2009. Aquatic arsenic: toxicity, speciation, transformations, and remediation. Environ. Int. 35, 743–759.
Sing, K.S., 1985. Reporting physisorption data for gas/solid systems with special reference to the determination of surface area and porosity (Recommendations 1984). Pure Appl. Chem. 57, 603–619.
Singh, A.P., Goel, R.K., Kaur, T., 2011. Mechanisms pertaining to arsenic toxicity. Toxicol. Int. 18, 87.
Singh, S.K., Townsend, T.G., Mazyck, D., Boyer, T.H., 2012. Equilibrium and intraparticle diffusion of stabilized landfill leachate onto micro- and meso-porous activated carbon. Water Res. 46, 491–499.
Wu, Z., Li, W., Webley, P.A., Zhao, D., 2012. General and controllable synthesis of novel mesoporous magnetic iron oxide@ carbon encapsulates for efficient arsenic removal. Adv. Mater. 24, 485–491.
Yu, X., Tong, S., Ge, M., Zuo, J., Cao, C., Song, W., 2013. One-step synthesis of magnetic composites of cellulose@ iron oxide nanoparticles for arsenic removal. J. Mater. Chem. 1, 959–965.